Jurnal Asiimetrik: Jurnal Ilmiah Rekayasa Dan Inovasi
Accredited "**SINTA 3**" based on the Decree of Dirjendiktiristek, Number: 225/E/KPT/2022
Volume 7 Number 1, January 2025, Page 13-20
Website : http://journal.univpancasila.ac.id/index.php/asiimetrik/

p-ISSN 2655-1861
e-ISSN 2716-2923

Erosive Wear Characteristics Analysis of High Chromium White Cast Iron Using Finite Element Analysis (FEA)

Analisa Karakteristik Keausan Erosif Besi Cor Putih Kromium Tinggi dengan *Finite Element Analysis* (FEA)

Riki Hendra Purba*, Deva Ihsan Khoirunas, James Julian, Fitri Wahyuni
Mechanical Engineering Department, Universitas Pembangunan Nasional Veteran Jakarta, Jakarta, Indonesia

Article information:

Received:
20/10/2024
Revised:
08/11/2024
Accepted:
25/11/2024

Abstract

Erosive wear often occurs on heavy machinery operating under extreme conditions. This research utilizes the Finite Element Analysis (FEA) method with the Cowper-Symonds strain rate model to analyze the erosion behavior of high-Cr cast iron (HCCI) under different impact angles and compare it to other materials of different characteristics, such as 6061-T6 Aluminium, GH4720Li Superalloy, and Stainless Steel 304 Annealed. A single particle erosion model was made for this study. The erodent particle size used is 0.7 mm in diameter, with the target material measuring 1 x 1 x 0.5 mm. The particle velocity is kept constant at 25 m/s. Based on the simulation results, it can be known that HCCI performs the best at every impact angle. Moreover, from the model's cross-section, it's evident that the material's stress concentration aligns with the direction of movement of the erodent particle. Therefore, it can be concluded that these factors, along with others such as contact time, plastic strain, and surface deformation lead to variations in surface mechanics.

Keywords: erosion model, Finite Element Analysis (FEA), high chromium white cast iron.

***SDGs*:**

Abstrak

Keausan erosi sering terjadi pada mesin berat yang beroperasi dalam kondisi ekstrem. Penelitian ini menggunakan *Finite Element Analysis* (FEA) dengan model *Cowper-Symonds strain rate* untuk menganalisa perilaku keausan erosif besi cor putih kromium tinggi (HCCI) pada tiga sudut *impak* yang berbeda dan dibandingkan dengan material lain seperti 6061-T6 Aluminium, GH4720Li Superalloy, dan Stainless Steel 304 Annealed. Sebuah model erosi partikel tunggal dibuat untuk penelitian ini. Diameter partikel eroden yang digunakan adalah 0.7 mm, dengan dimensi spesimen target sebesar 1x1x0.5 mm. Kecepatan impak partikel dijaga konstan pada 25 m/s. Berdasarkan hasil simulasi, dapat disimpulkan bahwa HCCI menunjukkan performa terbaik pada setiap sudut tumbukan. Selain itu, waktu kontak material *ductile* AL6061-T6 lebih besar. Akan tetapi, dari *cross-section* dapat diamati bahwa tegangan terpusat material mengikuti arah pergerakan partikel eroden. Faktor tersebut, bersama dengan faktor lainnya seperti waktu kontak, *plastic strain*, dan deformasi permukaan, menyebabkan variasi dalam karakteristik perubahan permukaan akibat gerak mekanik.

Kata Kunci: model erosif, *Finite Element Analysis* (FEA), besi cor putih kromium tinggi.

*Correspondence Author
email : rikihendrapurba@upnvj.ac.id

1. INTRODUCTION

Erosive wear occurs when the surface of a material experiences a collision with a particle moving at high velocity (Finnie, 1960; Zhang and Liu, 2023). Over time, the material's surface will undergo a reduction of material that causes degradation on that surface. Erosion often occurs in heavy machinery working under extreme conditions, such as gas turbines, aircraft engines, blast furnaces, industrial piping systems, and heavy equipment in mining industries (Shimizu *et al.*, 2019; Kusumoto *et al.*, 2024).

High chromium Cast Iron (HCCI) is the most used in heavy industries such as mining compared to other steel and cast-iron alloys. In mining environments, many equipment come into direct contact with materials that can cause erosion and abrasion, as seen in crushing and grinding mined products. HCCI has become the material of choice in this industry due to its low production cost and excellent resistance to wear and corrosion (Fernández and Belzunce, 2008; Pariente, Belzunce and Riba, 2008; Aziz, Shennawy and Omar, 2017; Prayogo and Setyana, 2021; Touhami *et al.*, 2023).

Developing erosion-resistant material is essential in increasing the lifespan of equipment, which would significantly reduce operating costs (Ngqase and Pan, 2020). Numerical analysis using Finite Element Method (FEM) is becoming a more common thing to do in research and development as technology advances. FEM analysis offers several benefits compared to analytical methods, such as lower cost and time (Patil and Jeyakarthikeyan, 2018).

Yaer et al., conducted numerical and experimental research on erosion in three superalloys types: GH720Li, GH738, and GH4169 (Yaer *et al.*, 2019). Sand particles (SiO_2) were chosen as erodents with a diameter of 700 μm traveling at speeds of 25 and 55 m/s and an impact angle ranging from 30 to 90 degrees. It was found that GH4720Li is the most erosion-resistant at low velocity and shallow angle of impact, while GH4169 is best at high impact velocity. The research also found that the simulation done closely matched the experimental works.

Zheng et al., investigated different parameters that affect erosive wear, such as impact angle, velocity, particle size, and material properties with multiple-particle 3D FEA analysis (Zheng *et al.*, 2017). This study uses Q345 as the target material. The results show that impact velocity and particle size have a linear correlation to the erosion rate. The erosion rate also increases as the velocity increase. Based on impact angle, this study shows a significant increase in erosion rate on impact angle between 20 to 50 degrees. Inaddition, Xiao et al., has conducted research with experimental and FEA analysis spheroidal carbide cast iron and suggests that harder and more brittle material tends to be more resistant to erosion at lower impact velocity and shallow angles (Xiao, Shimizu and Kusumoto, 2017).

Based on papers above, it can be said that the FEA can help researchers to determine the analysis of materials wear characteristics. However, eventhough the erosion behavior of HCCI has been chomprehensively evaluated by many scholars, the investigations were mostly conducted by the experimental method and just little attention is given to the numerical method. Therefore, this study proposes a single-particle FEA erosion model to understand more about the erosion behavior of HCCI material under different impact angles. This study also compares the erosion behavior of HCCI to other materials, such as 6061-T6 Aluminium, GH4720Li Superalloy, and Stainless Steel 304 Annealed to help the engineers in finding the best erosive wear resistance material.

2. METHODOLOGY

In this study, the research and simulation process are divided into several stages, as shown in Figure 1. The process begins with a literature review, where existing research and relevant theories are studied to establish a foundational basis for the study. Then, the simulation setup is prepared in the pre-processing stage, which involves creating the simulation model, defining the mesh, setting boundary conditions, and specifying material parameters.

With these preparations complete, the simulation can enter the solving phase using the Finite Element Method. In the post-processing phase, data from the simulation is collected and processed for analysis. A mesh convergence study is conducted to ensure that the simulation model is accurate. The validation step then assesses whether the simulation results align with experimental data or theoretical expectations. If the data obtained from the computational results is still invalid, the research will return to the pre-processing stage until the data is suitable and valid. The process concludes after the analysis, providing a rigorous and systematic workflow from preparation to final interpretation of results.

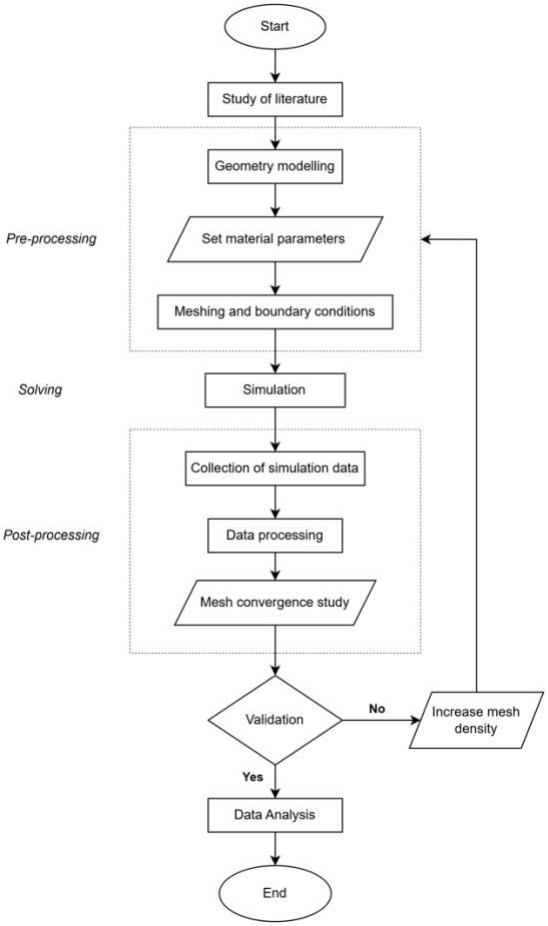

Figure 1. Research flowchart.

2.1. Materials

HCCI was chosen as the target material in this study using the Copper-Symonds strain rate material model. Three materials were chosen as a comparative variable for this study: 6061-T6 Aluminium, GH4720Li Superalloy, and Stainless Steel 304 Annealed. Sand particle (SiO2) was chosen as the eroding particle for this simulation. The material parameters used in this study are shown in Table 1.

Table 1. Material properties.

Materials	Density (kg/mm³)	Poisson Ratio	Young Modulus (GPa)	Yield Strength (GPa)
Al6061-T6	2.71e-6	0.33	68.95	0.287
GH4720Li	8.22e-6	0.35	156.75	1.1
HCCI	7.5e-6	0.28	175	1.296
SS 304	8.03e-6	0.29	193.74	0.163
SiO_2 (erodent)	2.2e-6	0.15	0.0731	

In Cowper-Symonds Strain Rate Model, The Yield Stress (σy) and Plastic Hardening Modulus (EP) can be calculated using Equations 1 and 2, respectively (Hernandez *et al.*, 2013).

$$\sigma_y = [1 + (\dot{\varepsilon}/C)^{\frac{1}{P}}](\sigma_0 + \beta E_P \varepsilon_P^{eff}) \quad (1)$$

$$E_P = \frac{E_{tan} E}{E - E_{tan}} \quad (2)$$

2.2. Simulation Geometry

In this study, it was created a three-dimensional FEA model to gain a better understanding of the erosion behavior of HCCI and three other materials, comparing them under three different impact angle variations. In the simulation, we used an erodent particle size of 0.7 mm, and the target material subjected to erosion had dimensions of 1x1x0.5 mm. It was consistently set the particle velocity at 25 m/s to eliminate the influence of impact velocity. The impact angles varied at 30, 60, and 90 degrees. The geometry of the simulation model is illustrated in Figure 2.

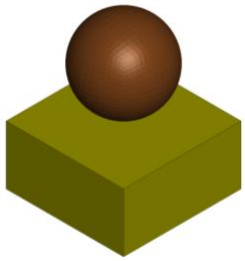

Figure 2. Simulation geometry.

2.3. Mesh Convergence Study

A Mesh Convergence Study is a standard method used in simulations to ensure that the number of mesh elements used does not influence the results (Patil and Jeyakarthikeyan, 2018). This test used four mesh densities: 62,500; 256,000; 500,000; 10^6 and $1.5x10^6$ elements. The test was conducted by comparing the maximum von Mises stress in the eroded material. The analysis indicated that as the number of mesh elements increased, the difference in maximum stress values across the models decreased. Consequently, a mesh density of 1 million was chosen for the simulations because it resulted in only a 0.73% difference in stress while requiring less simulation time than denser meshes. The detailed results of the mesh convergence study are presented in Table 2.

Table 2. Mesh convergence study results.

Mesh density	Maximum Stress (Gpa)	Error (%)
62,500	1.1183710098	
256,000	1.2531775236	10.76%
500,000	1.2954077721	3.26%
10^6	1.3098628521	1.1%
$1.5x0^6$	1.3194630146	0.73%

3. RESULTS AND DISCUSSION

In this study, it is essential to validate the simulation to ensure data accuracy. To do this, the simulation result was compared to data from a previous study by Yaer et al. (Yaer *et al.*, 2019). The validation process involved comparing the effective stress in the subsurface of the target material for each component of the x, y, and z axes. GH4720Li is used as the target material, with a particle impact velocity of 25 m/s and an impact angle of 90 degrees. As illustrated in Figure 3, the simulation data closely matches the results of the previous study. However, there are minor differences in the results, particularly at distances closer to the impact point (25 to 80 µm). These discrepancies maight be due to minor differences in the material parameters used in the simulation.

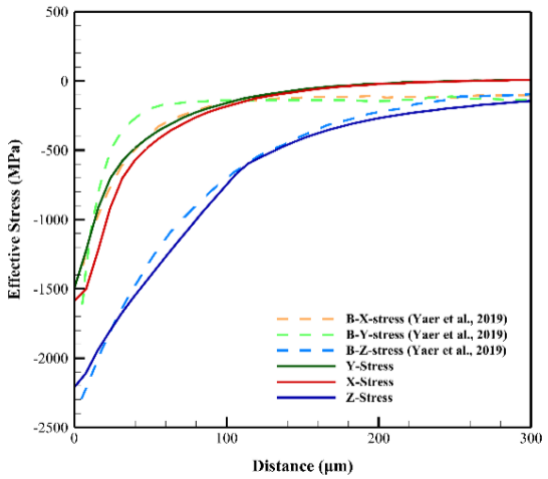

Figure 3. Simulation validation results.

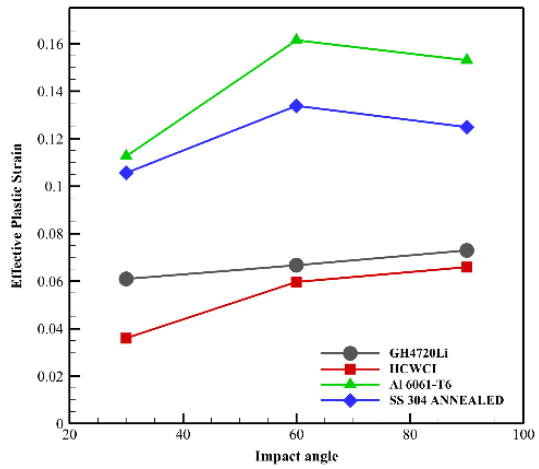

Figure 4. Effective plastic strain.

Figure 4 shows the maximum plastic strain of each material from the simulations conducted. The results indicate that harder and more brittle materials experience smaller plastic strains than the softer materials. For GH4720Li, the maximum plastic strain increases linearly with the rise in the impact angle. On all materials, the smallest plastic strain occurs at a 30-degree impact angle, then increases sharply when the angle is raised to 60 degrees for every material except GH4720Li. In more ductile materials, such as Aluminum 6061-T6 and Annealed Stainless Steel 304, the maximum plastic strain decreases at a 90-degree impact angle compared to a 60-degree impact angle. For brittle materials like HCCI and GH4720Li, there is a slight increase in effective plastic strain at the 90-degree angle.

A previous study by Xiao et al., found that the plastic strain directly correlates with the erosion behavior of a material (Xiao, Shimizu and Kusumoto, 2017). From this result, the HCCI would have the lowest erosion rate while the Aluminium 6061-T6 would have the highest.

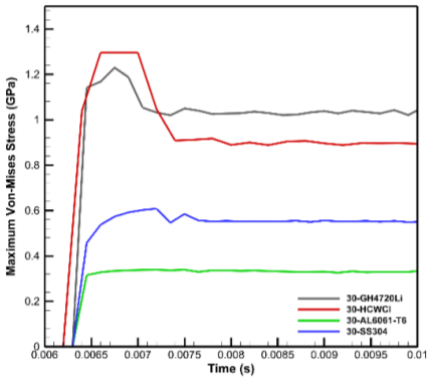

(a) Effective stress (v-m) at 30 degrees impact angle

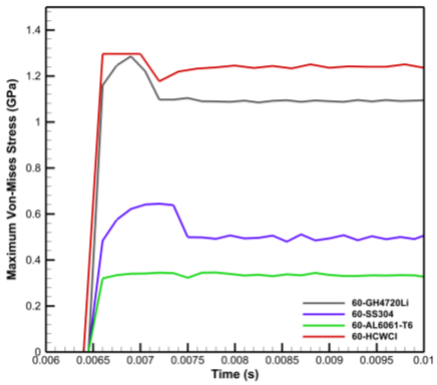

(b) Effective stress (v-m) at 60 degrees impact angle

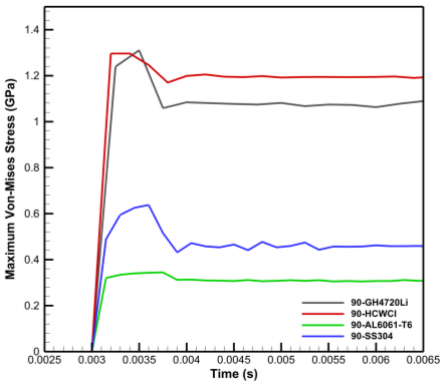

(c) Effective stress (v-m) at 90 degrees impact angle

Figure 5. Effective stress (v-m).

Figure 5 shows each material's maximum von Mises stress value over time under three different impact angles. The graph shows that all materials reach their yield stress upon impact. The stress levels in HCCI and GH4720Li materials decrease after the particles stop contacting the target material. At a 30-degree impact angle, as shown in Figure 5 (a), the stress level of HCCI decreases significantly after the impact, indicating some material removal from the surface. On Aluminium 6061-T6, the stress stays at its yield stress throughout the test on all impact angles. Stainless steel 304 behaves similarly to the Al 6061-T6 at an impact angle of 30 degrees, but on a higher impact angle, the stress level decreases after the impact, as shown in Figure 5 (b) and (c). The results show that the contact time between the eroding particle and the target material is longer at a shallow impact angle. From the results, AL6061-T6, the softest material, has the longest contact time at all impact angles, with HCCI having the least contact time. Then, the contact time decreases as the impact angle increases. This higher contact time would have an impact on erosion surface micromechanics.

In Figure 6, we can see the cross-sectional view of the simulation model when the particle makes its final contact with the target material. The von Mises stress distribution for each material can be analyzed from the contour given at different impact angles. At an impact angle of 30 degrees, the high-stress area is concentrated in the direction of the particle movement. This stress concentration, along with longer contact time compared to higher impact angles, tends to produce a cutting mechanism on the surface of the target material. Among the materials, HCCI (as shown in Figure 6 (a) has the smallest stress distribution area, followed by GH4720Li in Figure 6 (b) with a similar shape. AL6061-T6, being the softest material, experiences the highest stress level compared to other materials (as shown in Figure 6 (c)), and the area of concentrated stress is also the largest. SS-304 shows a behavior like AL6061-T6 but with smaller concentrated stress (Figure 6 (d)). In Figure 7 (a), the nodal displacement contour of HCCI at an impact angle of 30 degrees shows that the surface deformation is significantly less compared to a higher impact angle.

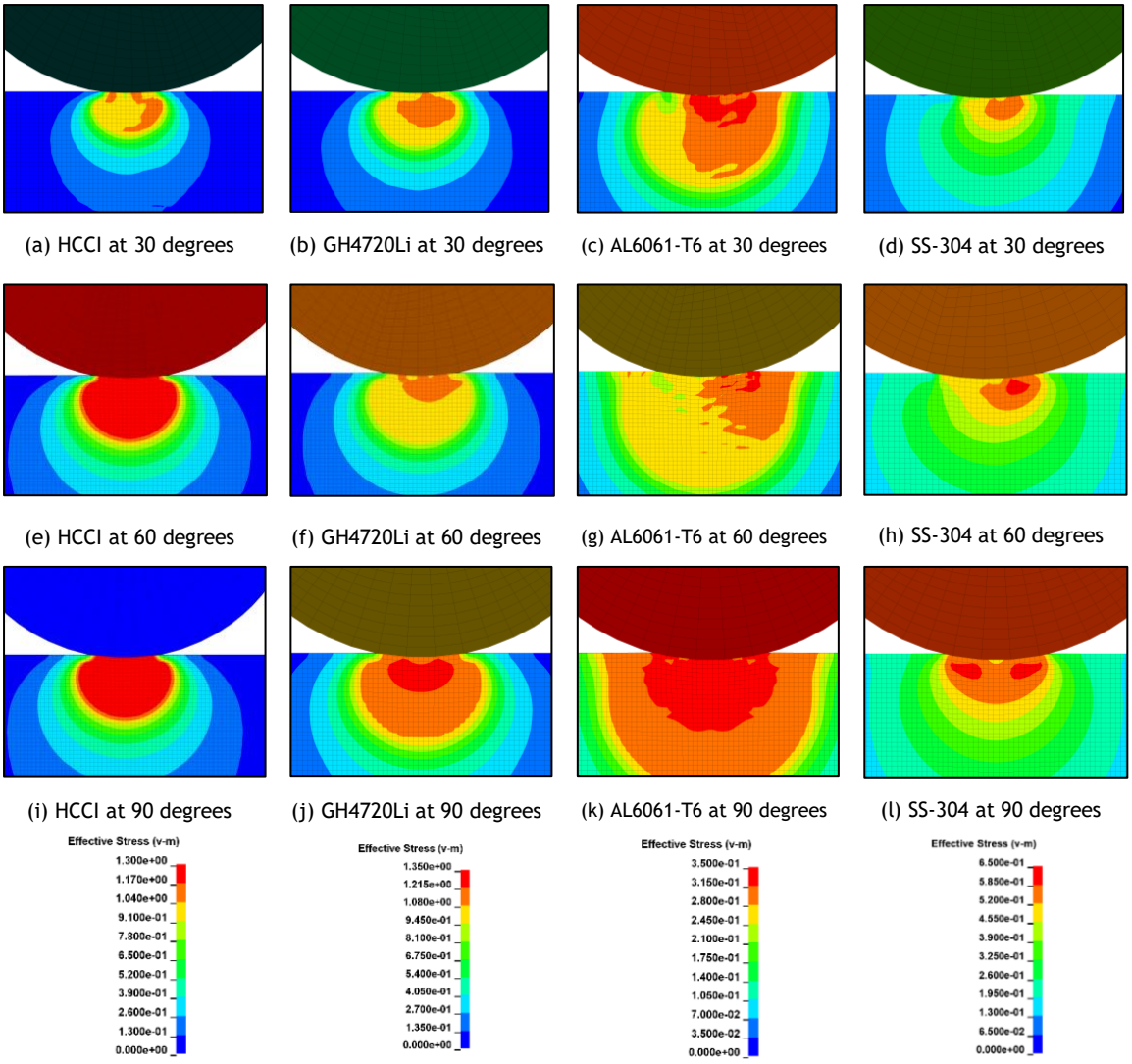

(a) HCCI at 30 degrees (b) GH4720Li at 30 degrees (c) AL6061-T6 at 30 degrees (d) SS-304 at 30 degrees

(e) HCCI at 60 degrees (f) GH4720Li at 60 degrees (g) AL6061-T6 at 60 degrees (h) SS-304 at 60 degrees

(i) HCCI at 90 degrees (j) GH4720Li at 90 degrees (k) AL6061-T6 at 90 degrees (l) SS-304 at 90 degrees

Figure 6. Cross sectional view of every material.

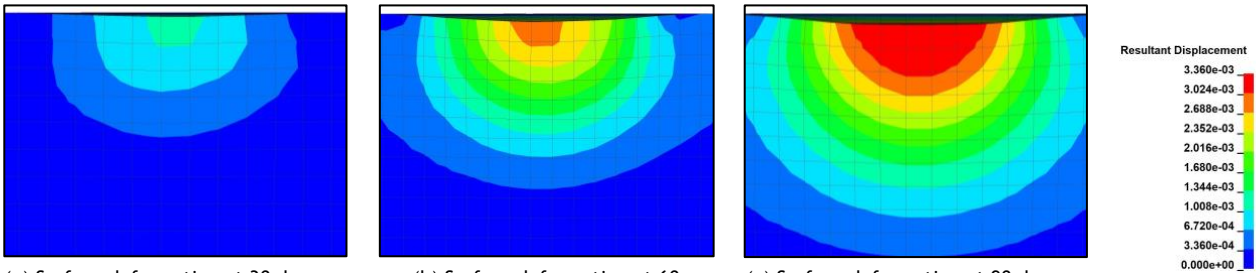

(a) Surface deformation at 30 degrees (b) Surface deformation at 60 degrees (c) Surface deformation at 90 degrees

Figure 7. Surface deformation of HCCI.

At an impact angle of 60 degrees, the effective stress area is more significant on all materials compared to a 30-degree impact angle. Figure 6 (e) shows the stress area distribution of HCCI at 60 degrees impact angle. At this angle, the stress is very concentrated, with a direction almost perpendicular to the material surface. The stress area is also significantly larger than at a 30-degree impact angle. This significant increase in effective stress results in a higher surface

deformation at this impact angle, as shown in Figure 7 (b). GH4720Li, as shown in Figure 6 (f), also has a similar stress distribution but with smaller concentrated stress. In AL6061-T6, the stress is distributed within a larger area with a high concentration of stress occurring in the direction of the particle movement. SS-304 has a similar stress concentration but with a lower magnitude than AL6061-T6, as shown in Figure 6 (g) and (h).

At a 90-degree impact angle, the materials experience the most significant stress concentration perpendicular to the material surface. At this angle, the stress distribution of HCCI remains similar to that observed at the 60-degree angle, with the stress concentration becoming more uniform, as shown in Figure 6 (i). GH4720Li has a larger stress distribution area than HCCI with a smaller maximum stress concentration, but the overall shape is still similar, as shown in Figure 6 (j). At this impact angle, the stress on AL6061-T6 and SS-304 is distributed over a larger area than at a shallower angle, as shown in Figure 6 (k) and (l), with a significantly larger high-stress area on the AL6061-T6. HCCI experiences the highest surface deformation at this impact angle, as shown in Figure 7 (c). At higher impact angles, indentations such as pits and craters are more likely to form on the material's surface.

4. CONCLUSION

The research examined how HCCI, GH4720Li, AL6061-T6, and Stainless Steel 304 Annealed respond to erosion at different impact angles using single-particle 3D Finite Element Analysis. The simulation results showed that HCCI experienced the lowest effective plastic strain at all impact angles. It was also noted that the effective strain on all materials was lowest at an impact angle of 30 degrees and then increased significantly as the impact angle reached 60 degrees. For HCCI and GH4720Li, the effective strain increased as the impact angle reached 90 degrees. On the other hand, the effective strain on AL6061-T6 and SS-304 decreased as the impact angle increased from 60 to 90 degrees.

The surface deformation of HCCI increased with the impact angle, while the contact time decreased with higher impact angles. It was also observed that softer materials like AL6061-T6 had a longer contact time, which could impact the surface micromechanics of erosion. The stress concentration within the materials was found to align with the direction of movement of the erodent particle. AL6061-T6 and SS-304 were noted to distribute stress over a larger area compared to HCCI and GH4720Li. These differences in stress concentration, contact time, deformation, and effective strain would lead to different surface mechanics.

The study concluded that the single-particle method still needs improvement to fully replicate real-world erosion phenomena. Therefore, further development of erosion simulation methods is necessary to better approximate erosion characteristics in HCCI and other materials.

REFERENCES

Aziz, Kh.A., Shennawy, M.E. and Omar, A.A. (2017) 'Microstructural Characteristics and Mechanical Properties of Heat Treated High-Cr White Cast Iron Alloys', *International Journal of Applied Engineering Research*, 12(4), pp. 4675–4686.

Fernández, I. and Belzunce, F.J. (2008) 'Wear And Oxidation Behaviour Of High-Chromium White Cast Irons', *Materials Characterization*, 59(6), pp. 669–674. Available at: https://doi.org/10.1016/j.matchar.2007.05.021.

Finnie, I. (1960) 'Erosion Of Surfaces By Solid Particles', *Wear*, 3(2), pp. 87–103. Available at: https://doi.org/10.1016/0043-1648(60)90055-7.

Hernandez, C. *et al.* (2013) 'A Computational Determination Of The Cowper-Symonds Parameters From A Single Taylor Test', *Applied Mathematical Modelling*, 37(7), pp. 4698–4708. Available at: https://doi.org/10.1016/j.apm.2012.10.010.

Kusumoto, K. *et al.* (2024) 'Effect Of Carbide Refinement On High Temperature Erosive Wear Behavior Of High Chromium White Cast Iron With Different Titanium And Carbon Additions', *Materials Today Communications*, 39, p. 109276. Available at:

https://doi.org/10.1016/j.mtcomm.2024.109276.

Ngqase, M. and Pan, X. (2020) 'An Overview on Types of White Cast Irons and High Chromium White Cast Irons', in *Journal of Physics: Conference Series. International Conference on Multifunctional Materials (ICMM-2019)*, Hyderabad, India: IOP Publishing, p. 012023. Available at: https://doi.org/10.1088/1742-6596/1495/1/012023.

Pariente, I.F., Belzunce, F.J. and Riba, C.R. y J. (2008) 'Mechanical Strength And Fracture Toughness Of High Chromium White Cast Irons', *Materials Science and Technology*, 24(8), pp. 981–985. Available at: https://doi.org/10.1179/174328407X213161.

Patil, H. and Jeyakarthikeyan, P.V. (2018) 'Mesh Convergence Study And Estimation Of Discretization Error Of Hub In Clutch Disc With Integration Of ANSYS', in *IOP Conference Series: Materials Science and Engineering. 2nd International conference on Advances in Mechanical Engineering (ICAME 2018)*, Kattankulathur, India: IOP Publishing, p. 012065. Available at: https://doi.org/10.1088/1757-899X/402/1/012065.

Prayogo, R.S. and Setyana, L.D. (2021) 'The Improvement of Wear and Impact Resistance of High Chromium White Cast Iron for Crusher', *Journal of Material Processing and Characterization*, 1(2), pp. 96–102. Available at: https://doi.org/10.22146/jmpc.68282.

Shimizu, K. *et al.* (2019) 'Microstructural Evaluation And High-Temperature Erosion Characteristics Of High Chromium Cast Irons', *Wear*, 426–427(Part A), pp. 420–427. Available at: https://doi.org/10.1016/j.wear.2019.01.043.

Touhami, R.C. *et al.* (2023) 'Wear Behavior and Microstructure Changes of a High Chromium Cast Iron: The Combined Effect of Heat Treatment and Alloying Elements', *Metallography, Microstructure, and Analysis*, 12(4), pp. 580–590. Available at: https://doi.org/10.1007/s13632-023-00976-w.

Xiao, L., Shimizu, K. and Kusumoto, K. (2017) 'Impact Angle Dependence of Erosive Wear for Spheroidal Carbide Cast Iron', *Materials Transactions*, 58(7), pp. 1032–1037. Available at: https://doi.org/10.2320/matertrans.F-M2017816.

Yaer, X. *et al.* (2019) 'Surface Deformation Micromechanics Of Erosion Damage At Different Angles And Velocities For Aero-Engine Hot-End Components', *Wear*, 426–427, pp. 527–538. Available at: https://doi.org/10.1016/j.wear.2018.12.054.

Zhang, J. and Liu, H. (2023) 'Effect Of Solid Particles On Performance And Erosion Characteristics Of A High-Pressure Turbine', *Energy*, 272, p. 127185. Available at: https://doi.org/10.1016/j.energy.2023.127185.

Zheng, C. *et al.* (2017) 'Finite Element Analysis On The Dynamic Erosion Process Using Multiple-Particle Impact Model', *Powder Technology*, 315, pp. 163–170. Available at: https://doi.org/10.1016/j.powtec.2017.04.016.